

# Ring Laser Gyros: Improving Precision and Accuracy Through Soft-Core Processor-Based Active Current Balance Control Approach- Simulation and Implementation Results

Thoudoju Sreeramulu<sup>1</sup>, Prof. Lavadya Nirmala Devi<sup>2</sup>, Dr. Avunuri Ramchander Rao<sup>3</sup>, Dr. Gangalakurti Laxminarayana<sup>4</sup>

<sup>1</sup>Department of Electronics and Communication Engineering,  
University College of Engineering, Osmania University,  
Hyderabad-500007, Telangana, India.  
E-mail: t\_sreeram@hotmail.com

<sup>2</sup>Department of Electronics and Communication Engineering,  
University College of Engineering, Osmania University,  
Hyderabad-500007, Telangana, India.  
E-mail: nirmaladevi@osmania.ac.in

<sup>3</sup>Directorate of Laser Systems, Research Center Imarat,  
Defence Research and Development Organization,  
Hyderabad-500069, Telangana, India.  
E-mail: arrao@rcilab.in

<sup>4</sup>Directorate of Laser Systems, Research Center Imarat,  
Defence Research and Development Organization,  
Hyderabad-500069, Telangana, India.  
E-mail: g.lnarayana@rcilab.in

**Abstract**—In this article, we intend to demonstrate on digital active current control in ring laser gyros (RLG). The specific source errors that effect the performance of laser gyro is discussed. This work proposes a system of digital detection and control system to address deficiencies of the conventional analog circuits. The hardware framework is constructed using the Field Programmable Gate Array (FPGA) and the required analog interface, which incorporates driving and acquisition circuitry for the specific physics of gyros. The software flow is provided in full and uses the parallel PI (proportional-integral) control algorithms. The outcomes demonstrate that the precision of anode currents are accurately controlled within  $\pm 0.1\mu\text{A}$  along with cathode voltage, demonstrating that the performance of the digital system is superior to that of analog circuits, which will be very beneficial for the laser gyro application. The simulation results prove that the proposed approach has good result of balancing anode currents, meanwhile, it makes the sensor a good dynamic performance. In both anodes, the experimental findings are contrasted with balanced and unbalanced currents. The optimal constant current is obtained from the remarkable agreement between simulated and experimental results.

**Keywords** - Bias, Current balance, Digital detection and control, Ring laser gyro.

## I. INTRODUCTION

The ring laser gyros (RLG) are proven technology and are capable to detect the angular rotation rate with respect to its plane relative to the inertial frame. Its fundamental operation explores the Sagnac effect [1-4] the rotation rate causes the optical length [5, 6] of the sensor cavity as seen by the two oppositely travelling or the counter-propagating optical beams in the laser are different. This difference in travelling shifts directly into the optical frequency shift between the two counter

propagating beams and is proportional to the angular rotation rate based on the Eq. (1). Where  $\Omega$  is the angular velocity,  $L$  is the perimeter of the ring sensor cavity,  $\lambda$  is the laser wavelength

$$\Delta\nu = \frac{4A \cdot \Omega}{\lambda L} \quad (1)$$

and  $A$  is the area vector (perpendicular to ring surface). The shift which is called as Sagnac frequency and can be measured by allowing the two oppositely travelling beams beat. Null shift

[1, 7] occurs when both frequency differences are skewed. In the active laser medium, a phenomenon known as Langmuir flow [1, 7] is the main cavity anisotropy that causes null shift errors. If no null shift is to be noticed, the typical solution to this concern is to accurately match the discharge currents [8, 9] in both legs. A comparable null shift of 0.0066 deg/h [7] resulted from a 1  $\mu$ A imbalance in the two currents.

Though ring laser gyro uses zerodur or quartz as a base material to lessen performance uncertainty brought on by thermal impacts, the RLG also produces bias drift due to the current unbalancing of anodes.

This paper proposes new system that has a lower footprint than the old analog control system, which mostly uses analog circuitry, and it can adjust work parameters flexibly through software.

## II. WORKING PRINCIPLE OF RLG AND OUTPUT PULSES

### A. Working Principle

The ring laser gyro measures the angular rotation using a light from the laser. A square-shaped helium-neon laser emits dual light beams, one of which moves clockwise and the other counterclockwise. High voltage is used to ionize the helium-neon combination at low pressure to create a glow discharge [7], which is where the creation of light beams of lasing takes place. The clockwise and counterclockwise light beams are created by the lasing's light being reflected around the square by mirrors at each of its four corners.

In order for the cavity path length [5, 6] to be an integral multiple of the laser wavelength with the highest peak power, it is carefully monitored and modified.

A fringe pattern made up of alternately dark and bright stripes are produced when the laser beam frequencies vary. Photodiodes detect the rate and motion direction of the fringe pattern [10, 11, 12]. The size and direction of the gyro's spin are indicated by the frequency and relative phase of the two diode outputs.

The little frequency change between the laser beams causes beam coupling at slow rotation speeds. Hence both frequencies lock together [13] to a single false value in this way. A piezoelectric dither motor [15] is utilized to shake the laser block through the lock-in zone [20, 21] to counteract this effect. Dither vibration averages to zero. There is no net inertial rotation produced. The laser block casing vibrates from the dither motor, which also emits a perceptible hum.

### B. Gyro Output Pulses

At very low input rates, the RLG experiences a phenomena called lock-in. The inability of the gyro to sense the input rotational rates at low inputs is called lock-in. To get rid of this lock-in, the gyro is subjected to to-and-fro vibration which is called as mechanical dithering [13, 14, 15] wherein the gyro is

fixed to rigid body. In addition to mechanical dithering, a component called Pseudo Random Noise (PRN) [14] is also introduced into the amplitude of dither, ensuring that the gyro is brought to nearly continuous rotation rate all the time.

The supporting signal processing electronics of the gyro converts the incremental rate into a digital pulses wherein each pulse is weighed with the scale factor of the gyro. These pulses are counted into a digital words after processing and it consists of incremental angle due to the rate input motion and as well as rate due to sinusoidal dither motion. The sinusoidal dither motion and random noise components are removed or filtered out by using the digital filtering technique [10] whose pass band frequencies come under all possible rotation rate input of the ring laser gyro. The dither motion rate is removed in real time by applying 2 stage FIR filters with optimum filter length having rectangular window. Just by varying minimal coefficients in the memory, one can achieve required noise characteristics and the gyro bandwidth.

## III. CURRENT BALANCE PHENOMENA

As stated earlier, ring laser gyro measures the rotation rate around the ring's sensitive axis as a function of the beat frequency, or difference in frequency between the two counter-propagating beams. Such counter-propagating beams are created via a procedure that typically involves a DC discharge of electricity in an appropriate Helium-Neon mixer gain medium. The wall effect and subsequent charging of the wall region are caused by this electrical discharge [1]. This disrupts the pressure balance in that area and interacts with the moving medium which is called as Fresnel-Fizeau drag [1], causing a frequency shift in the counter-propagating beams. As a result, the optical length of the beam moving in the direction of flow is different from the optical length of the beam moving in the flow's opposite direction. The output signal therefore has a component known as Fresnel-Fizeau bias, since the flow causes a beat frequency between the counter-propagating beams that is not caused by the rotation of the ring route. To counteract this bias, the configuration of gyro is made in such a way that the two balanced electrical discharges are directed in opposite directions [7]. As a result, even when two electrical discharges are not exactly balanced, a net bias still develops because of the uneven drag.

It has been observed that a systematic change in the magnitude of the bias produced by the optical bias occurs as the gyro heats up. This change is attributed to the temperature sensitivity as the gyro heats up and it has been noticed that there is a consistent shift in the magnitude of the bias which in turn caused by the optical bias. The temperature sensitivity of the reflecting optical components [1] inside the gyro is responsible for this shift. For several hours after the gyro is powered, the magnitude of the bias decreases over time due to this self-

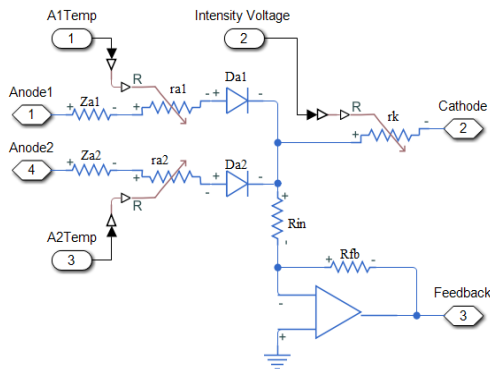


Figure 1. Equivalent RLG anode-cathode behavior model with intensity feedback.

heating. The extent of this shift is equivalent to a reduction in beat frequency of approximately 600 Hz over a 5-hour run at room temperature. With the help of a current regulator circuit, a constant amount of current is provided to make up for the change in bias. Temperature sensors are used throughout the electronics assembly to steady the gyro in addition to compensating for the effects of temperature, and regulator circuits use precision reference voltage and precision thin film resistors.

#### IV. SIMULATION OF INTENSITY CONTROL AND CURRENT BALANCE CONTROL LOOPS

##### A. Simulink Model

In terms of cathode voltage and anode currents, the simulation goal is to realize control dynamics. Figure 1 shows the equivalent RLG anode-cathode Simulink behavior model

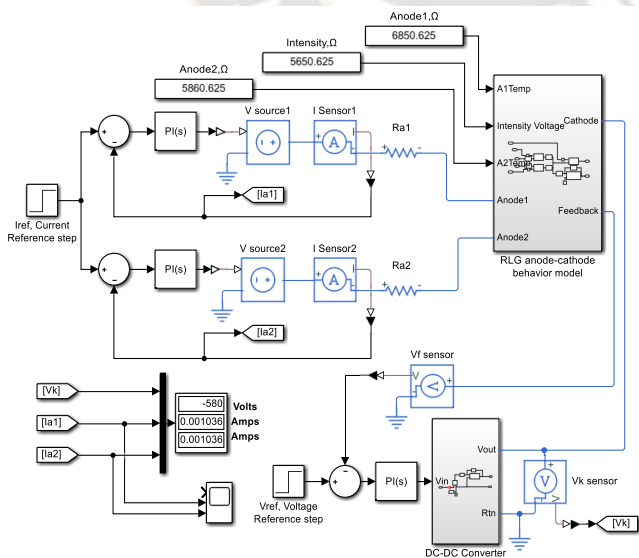


Figure 2. Simulink model for intensity and current balance control.

with intensity feedback. The ring laser gyro is modelled as a high-voltage diodes Da1 and Da2 with cathodes connected to each other and both the anodes are given equivalent series impedances Za1 and Za2, both of which are about 400 kΩ. A

variable resistor rk (74 kΩ) is attached to simulate the variations in laser beam intensity in the ring laser gyro.

In addition to this, a variable series resistances ra1 and ra2 are also connected to each anode, so that the current differences can be introduced on anodes on-fly by varying them. All variable resistor wiper terminals use unitless Simulink input signals transformed into a physical signals. This physical signal wipes the resistor according to Simulink input. In order to mimic the intensity amplitude found in the sensor, a small amount of voltage from the cathode is additionally obtained as feedback using an op-amp as an attenuator. This voltage is proportional to the amplitude of intensity.

Figure 2 shows the simulation of intensity and current balance control loops in Simulink. The DC-DC converter is an ideal converter that generates the negative high voltage output which is required for cathode. The negative voltage to cathode is an inherent requirement of RLG [1, 7]. The optimum cathode voltage and anode currents are practically recorded from an open loop test and then these values are applied in this model. The voltage and current reference steps for cathode and anode control loops are taken as  $V_{ref} = 1.19$  volts and  $I_{ref} = 1.036$  mA respectively which represents the actual block requirements of laser intensity and currents in anodes. The ballast resistors Ra1 and Ra2 are used to limit the currents in anodes during the firing of He-Ne gas towards discharge followed by lasing. Both resistors are found to be 82 kΩ by using an actual gyro before being used in this model to determine which ballast resistors are to be employed when taking a discharge. Simulink Simscape electrical blocks are used for this simulation.

In the intensity control loop Simulink model, a step voltage is set and then the error is derived by taking feedback from RLG. This error is fed to PI controller [16, 22] with tuned proportional and integral constants as 9 and 128 respectively. The output of PI controller is given to the DC-DC converter to generate the negative high voltage that drives the cathode of sensor block. Vksensor and Vfsensor senses the voltage at output of DC-DC converter and feedback voltage from RLG respectively. As Vfsensor output is physical signal, a PS-simulink block is used here to get the unitless Simulink output. Vksensor output is a physical signal that transforms into unitless Simulink which is used for monitoring.

The outputs of PI current controllers converts the unitless Simulink signal to its respective physical signals and drives Vsource1 and Vsource2 which drives anode1 and anode2. Isensor1 and Isensor2 are used to sense the currents in both the anodes. The physical signal is transformed into unitless Simulink signal and is taken as a feedback to control the anode currents. Both PI controllers are optimally tuned to proportional and integral constants having 78 and 1895 respectively. The anode resistances ra1 and ra2 are not set equal, before the model

is simulated. These variable resistance values for anode1 and anode2 are taken as 6.85 kΩ and 5.86 kΩ respectively.

Figure 3 shows that cathode voltage settles to -580 volts for a given Vref of 1.19 volts to get the same feedback. The initial cathode voltage is adjusted to -200 volts as the block should have minimum voltage to sustain the laser itself. Similarly both the anode currents settle to 1.036 mA equally. Hence, irrespective of variations in anodes due to temperature or for any other reason, the currents in anodes remains constant.

**B. Multisim Hardware Simulation With Precision Instrument Difference Amplifier**

The hardware simulation is carried out in multisim software using the findings of the simulation done in simulink. The hardware configuration using a precision instrument difference amplifier AD8479, with a very large input common-mode voltage range is shown in Figure 4. With the aid of the difference amplifier, the anode currents are precisely measured with differential signals even when large common-mode voltages of up to 600 Volts are present and features inputs that are 600 Volts transient common-mode or differential mode protected. It only senses the currents in both the anodes by configuring amplifier in the differential mode with ±15volts supply voltage. The anode2 impedance Za2 is slightly varied to 95% of Za1, where R1, R2, R3, and R4 are chosen as 1KΩ each,

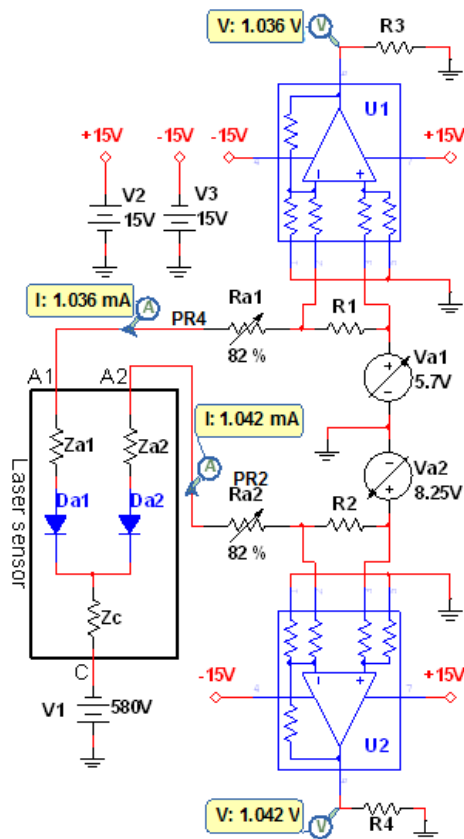


Figure 4. Hardware simulation of current sensing circuit with difference amplifier using Multisim.

so that drop across R1 and R2 reflects the current in that resistor and so the output of difference amplifier. It can be observed from Figure 4, that current in anode1 is 1.036mA and the same is reflected at output of op-amp and across the resistor R3 as voltage. Similarly, the current in anode2 is 1.042mA and the same is reflected at output of op-amp as a voltage across the resistor R4. Voltage sources Va1 and Va2 are manually varied to adjust the currents in anodes, but in real conditions the PI controller automatically tunes the required control voltage.

**V. HARDWARE AND SOFTWARE REALIZATION**

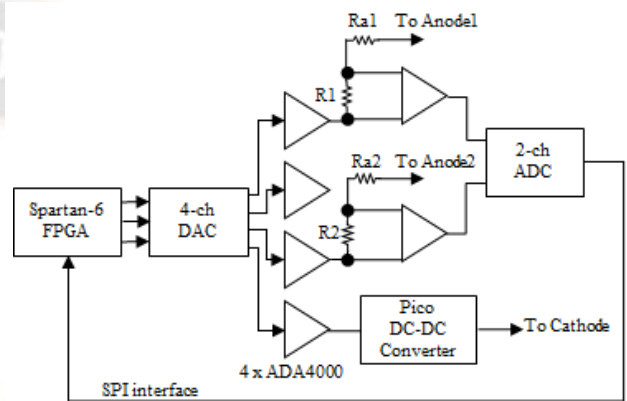


Figure 5. Block diagram of proposed hardware with difference amplifier.

**A. Hardware Realization**

A schematic is made in Orcad software and its equivalent block diagram is shown in Figure 5, and then it is brought into hardware PCB for implementing in real time. Current sense resistors R1 and R2 are selected as ultrahigh precision resistors

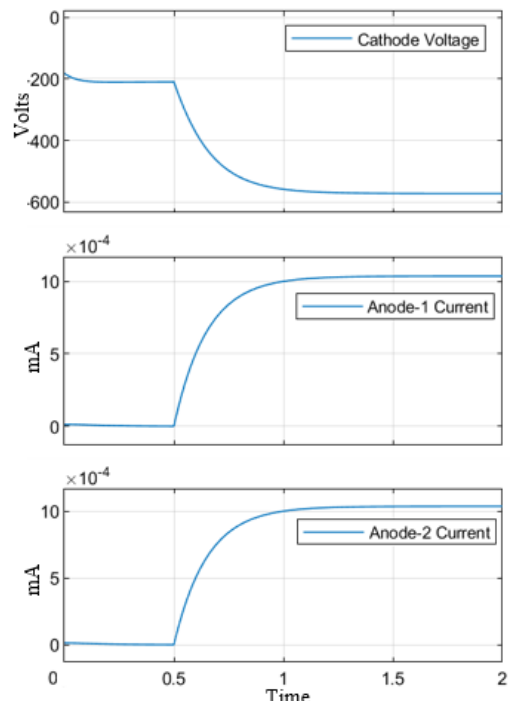


Figure 3. Step response of intensity and current balancing loops.

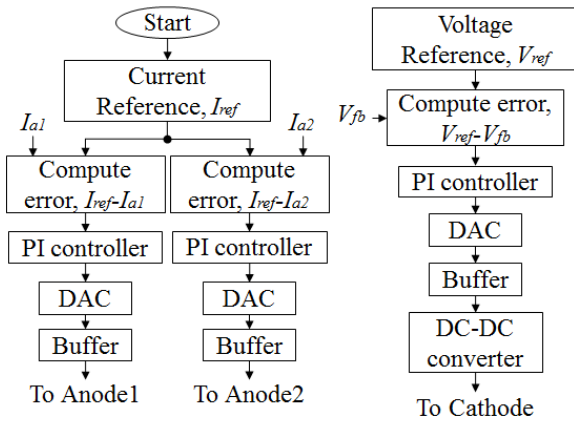


Figure 6. Flow chart for software implementation.

with high temperature coefficient of  $\pm 0.2\text{ppm}/^\circ\text{C}$  and tolerance of  $\pm 0.01\%$  having temperature range from  $-55^\circ\text{C}$  to  $+125^\circ\text{C}$ . In addition to that, the part numbers for a series resistances  $R_{a1}$  and  $R_{a2}$  are also selected with temperature coefficient of  $\pm 10\text{ppm}/^\circ\text{C}$  and tolerance of  $\pm 0.1\%$  having temperature range from  $-55^\circ\text{C}$  to  $+155^\circ\text{C}$ .

The logic control signals from Spartan-6 FPGA drives 4 channel DAC. The logic module is written in verilog hardware description language, synthesized, translated, mapped, place & routed, generated the bit file and then dumped into the FPGA. The data and control signals provided to the DAC produce analog signals needed to regulate the intensity and anode currents. To isolate the high voltage coming toward the DAC, the precision op-amp (ADA4000) with appropriate gain is also used. The hardware implemented consists of a DC-DC converter and also difference amplifier. The voltage drop across  $R_1$  and  $R_2$  are sent to two-channel ADC using difference amplifiers. The output of the ADC is fed back to FPGA for digital processing.

The FPGA's Microblaze softcore processor operates at a 100MHz clock speed. To exchange data between a programmable logic and processing system, the user-configurable AXI Lite interface is used. The interface logic module for ADCs and DACs are implemented in programmable logic and control algorithms are implemented in the Microblaze processing system. In addition to this, the user configurable peripheral IPs like, UART16650, AXI interrupt controller, AXI timer, local memory bus and block RAMS are used.

### B. Software Realization

Figure 6 represents the software implementation in micoblaze processor.  $I_{ref}$  and  $V_{ref}$  are desired reference digital equivalent values of anode currents and cathode voltage. These values are achieved by tuning the PI controller [16, 22] in open loop condition along with sensor and then stored in the flash memory. The Eq. (2), Eq. (3), and Eq. (4) represents the fixed

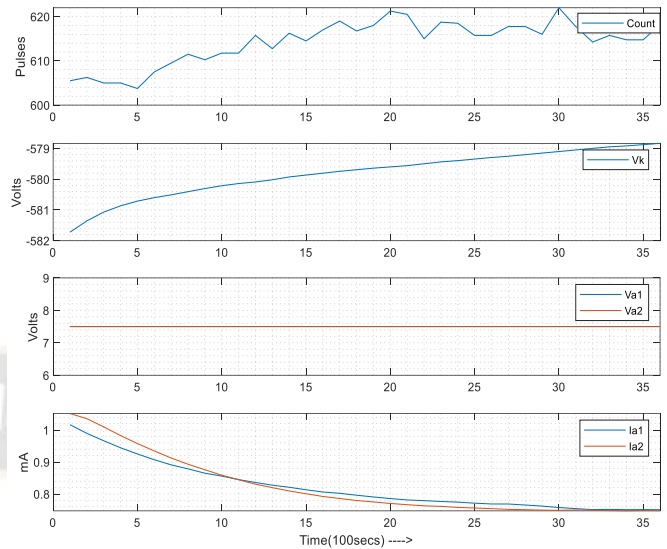


Figure 7. Open loop anode1 and anode2 current test results.

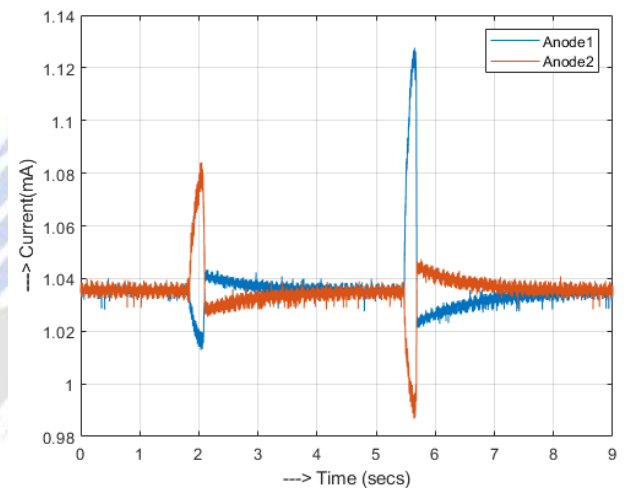


Figure 8. Settling of anode currents to 1.036 mA after manual disturbance.

point discrete PI controllers implemented in softcore Microblaze processor

$$V_{A1}[n] = V_{A1}[n - 1] + G_1(I_{ref} - I_{a1}) \quad (2)$$

$$V_{A2}[n] = V_{A2}[n - 1] + G_2(I_{ref} - I_{a2}) \quad (3)$$

$$V_k[n] = V_k[n - 1] + G(V_{ref} - V_{fb}) \quad (4)$$

Where  $V_{A1}[n]$ ,  $V_{A2}[n]$ , and  $V_k[n]$  are discrete present samples of anode1, anode2, and cathode voltages respectively.  $V_{A1}[n - 1]$ ,  $V_{A2}[n - 1]$ , and  $V_k[n - 1]$  are discrete previous samples of anode1, anode2, and cathode voltages respectively.  $G_1$ ,  $G_2$ , and  $G$  are tuned gain parameters of anode1, anode2 and cathode respectively.

The errors  $I_{ref}-I_{a1}$  and  $I_{ref}-I_{a2}$  are fed to the PI controller and then passed on to the DAC followed by the analog buffer. It is then fed to anode1 and anode2. Buffers drive the anodes in

0-15Volts range. The error  $V_{ref}-V_{fb}$  are provided to the PI controller, fed to the DAC to obtain the proportional analog signal, and after buffering, given to the DC-DC converter to drive the cathode of RLG.

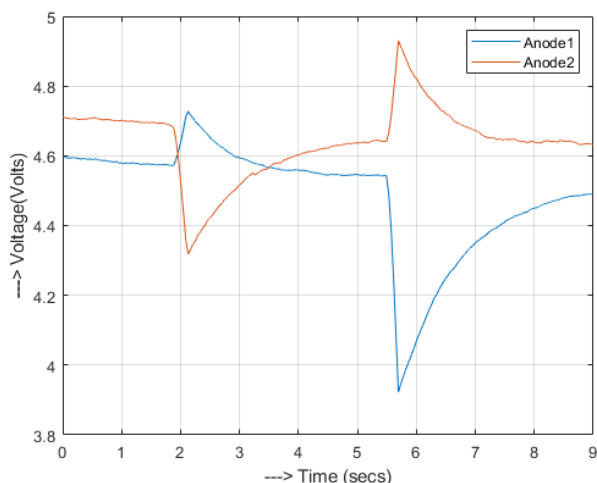


Figure 9. Respective voltage changes required to balance the currents to 1.036 mA.

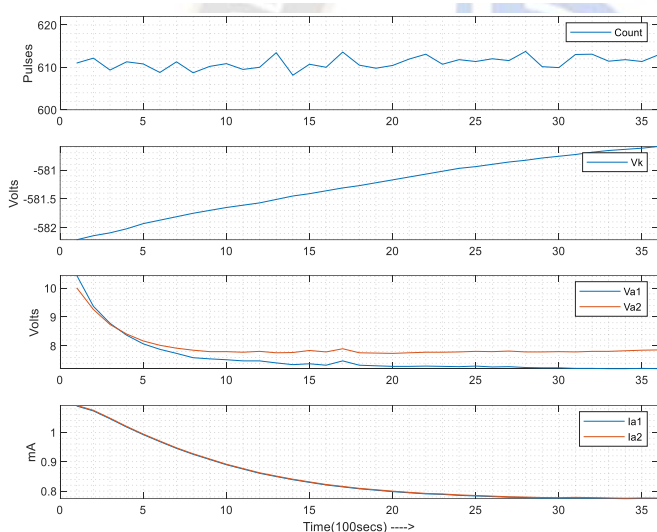


Figure 10. Closed loop anode1 and anode2 current test results.

## VI. EXPERIMENTS

The test setup is made by connecting the controlled signals to cathode and anodes of RLG. The test runs are given for an hour each without and with anode current balancing. As mentioned earlier, the RLG output (pulses) is accumulated for 100 seconds, and the remaining parameters are averaged and plotted over that time.

Figure 7 depicts the test results for both open loop anodes and closed loop cathode. The open loop anode voltages are fixed at 7.5 volts each. It can be seen that currents are not equal initially and eventually falls, where as count drifts [1, 17]. This is because the anode currents are not equal.

Close loop anode experiments were carried out further. Figure 8 and Figure 9 shows the manual disturbances of anode currents and voltages in a closed loop situation, respectively. It can be seen that the currents draw closer, back to its actual values (1.036mA) where its respective voltages are different. Figure10 shows the test run for 1 hour in close loop condition. It is clearly visible that the anode currents are very close to each other with a  $\pm 0.1\mu A$  error. During this 1 hour, the currents at any given time are equal in both the anodes and continues for the complete duration of time. During the test run the anode currents settle to 0.78mA where the anode voltages differ by 0.8 volts. It is the required anode voltages at which the anode currents are equal.

## VII. CONCLUSION

Digital and advanced computerized innovation has helped with all transformations by simplifying lives, quicker, better, viable and more charming. This study developed a novel approach of digital active current balance control system for RLG in digital domain and incorporated the crucial analog interface with the extremely capable processing Spartan-6 FPGA. This study has simulated the concept of anode current balancing in Simulink and then the hardware is simulated with difference amplifier in Multisim software and brought into a real working PCB electronics. The software control methods are used in Microblaze softcore processor in FPGA. The legitimacy of the framework, which performs better compared to customary simple circuits and has great application possibilities for RLG, has been affirmed by experimental results. These sensors have higher application [18, 19] demand in inertial navigation of missiles and aircrafts.

## ACKNOWLEDGMENT

The Technology Director, DLS, RCI, DRDO, Hyderabad is acknowledged by the authors with their heartfelt gratitude for helping to make the research work possible.

## REFERENCES

- [1] Frederick Aronowitz, "Fundamentals of the Ring Laser Gyro", in Optical gyros and their application, BP 25, 7 Rue Ancelle, F-92201 Nueilly-Sur-Seine Cedex, France, 1999, pp. 3.1-3.15.
- [2] Woo-Seok Choi, Kyu-Min Shim, Kyung-Ho Chong, Jun-Eon An, Cheon-Joong Kim and Byung-Yoon Park. Sagnac Effect Compensations and Locked States in a Ring Laser Gyroscope. Optical Sensors.3 February 2023. DOI: 10.3390/s23031718.
- [3] I. L. Paiva, R. Lenny, and E. Cohen. Geometric phases and the Sagnac effect: Foundational aspects and sensing applications. Advanced Quantum Technologies. 15 Jan 2022. DOI: 10.1002/qute.202100121.
- [4] Bhadra, A., Ghose, S. & Raychaudhuri, B. A quest for the origin of the Sagnac effect. The European Physical Journal. J. C 82, 649 (2022). DOI:10.1140/epjc/s10052-022-10620-6.

- [5] Tevfik Ozan Fenercioğlu and Tuncay Yalçinkaya. Computational-Experimental Design Framework for Laser Path Length Controller. *Sensors*, Jul 31, 2021. DOI: 10.3390/s21155209.
- [6] P.F.Lan, Y.Z.Liu, J.L.Wang, M.H.Zhang. Research and improvement of path length control configuration for laser gyroscopes. An article. Volume 34. pp: 161-165. Jan 2013. DOI:10.5768/JAO201334.0107004.
- [7] Modular Ring Laser Gyro, by Joseph E. Killpatrick and Dale Berndt. (2001, March 27), Patent 6208414B1.
- [8] Faucheux Marc, D.Fayoux, J.J. Roland. Ring Laser Gyro, December 2000, *Journal of Optics* 19(3):101. DOI:10.1088/0150-536X/19/3/001.
- [9] Angela D. V. Di Virgilio, Nicolò Beverini, Giorgio Carelli, Donatella Ciampini, Francesco Fusco & Enrico Maccioni. Analysis of ring laser gyroscopes including laser dynamics. *The European Physical Journal C*, volume 79, Article number: 573 (2019). DOI:10.1140/epjc/s10052-019-7089-5.
- [10] Loren W. Richardson, "Ring laser gyro applications for high accuracy pointing and tracking in space", SPIE's International Symposium on Optical Engineering and Photonics in Aerospace Sensing, Orlando, FL, USA, 1994.
- [11] G. Gilster, "High accuracy performance capabilities of the military standard ring laser gyro inertial navigation unit", 1994 April, 1994, PLANS'94.
- [12] Mario. N. Armenise, C. Ciminelli, F. Dell'Olio, and V. M. N. Passaro, "He-Ne and Solid-State Ring Laser Gyroscopes", in *Advances in Gyroscope Technologies*. 1<sup>st</sup> ed, Springer Berlin, Heidelberg, 2011, ch. 3, pp17-28.
- [13] Zhenfang Fan, Hui Luo, Shaomin Hu, Guangzong Xiao, "Research on lock-in correction for mechanical dithered ring laser gyro", *Optical Engineering*, Vol.50, No. 3, 034403, 1 March 2011.
- [14] Zhenfang Fan, Hui Luo, Guangfeng Lu, Shaomin Hu, "Direct dither control without external feedback for ring laser gyros", in *Optics and Laser Technology*. Changsha, China, Vol 44, Issue4, June 2012, pp 767-770.
- [15] S M Yang and J S Chiu, "Dither-motor design with concurrent sensing and actuating piezoelectric materials" *Smart materials and Structures*, vol 3, no 2, IOP publishing, 1994. DOI 10.1088/0964-1726/3/2/22.
- [16] Yang Jianqiang, Jia Xueqing, Yuan Baolun 2010, March 27-29. Digital Detection and Control System for Ring Laser Gyro. ICACC.
- [17] Microprocessor controlled ring laser gyro power control system, by Joseph E. Killpatrick and Dale Berndt. (2008). Patent Number EP0760934B1.
- [18] G. Satheesh Reddy and V.K. Saraswat. Advanced Navigation System for Aircraft Applications. *Defence Science Journal*, Vol. 63, No. 2, March 2013, pp. 131-137, DOI: 10.14429/dsj.63.4254.
- [19] Li Z, Zhang L, Wu. K. Filter Design for Laser Inertial Navigation System Based on Improved Pigeon-Inspired Optimization. *Aerospace* 2023, 10, 63. DOI: 10.3390/aerospace10010063.
- [20] Merzlikin, A.M., Puzko, R.S. Mode locking suppression in a magneto-optical gyro. *Scientific Reports* 10, 19490 (2020). DOI: 10.1038/s41598-020-76331-8.
- [21] Yuan-zheng, Jing-xian, Yang-hua, Pei-feng, Lock-in Zone Controlling for Ring Laser Gyro. *ACTA PHOTONICA SINICA*. 2010. Volume 39. pp:781-784. DOI: 10.3788/gzxb20103905.0781.
- [22] Jianqiang Yang, Dan Liao, Meng Gao. A new method of gain stabilization and its fuzzy-PID control algorithm for ring laser gyro. Jan 2010. International conference on computer Automation and Engineering. DOI:10.1109/ICCAE.2010.5451655.